January 2008

The Effect of Ca, Sr, and Ba Doping on the Ionic Conductivity and Cathode Performance of $LaFeO_3$

Fred Bidrawn
University of Pennsylvania

S. Lee
Korea Institute of Energy Research

John M. Vohs
University of Pennsylvania, vohs@seas.upenn.edu

Raymond J. Gorte
University of Pennsylvania, gorte@seas.upenn.edu

The Effect of Ca, Sr, and Ba Doping on the Ionic Conductivity and Cathode Performance of $LaFeO_3$

Abstract

The influence of ionic conductivity on the performance of solid oxide fuel cell cathodes was studied for electrodes prepared by infiltration of 40 wt % $La_{0.8}Ca_{0.2}FeO_3$ (LCF) $La_{0.8}Sr_{0.2}FeO_3$ (LSF) and $La_{0.8}Ba_{0.2}FeO_3$ (LBF) into 65% porous yttria-stabilized zirconia (LSZ). The ionic conductivities of LCF, LSF, and LBF, measured between 923 and 1073 K using permeation rates in a membrane reactor, showed that LSF exhibited the highest ionic conductivities, followed by LBF and LCF. When electrodes were calcined to 1123 K, the performance characteristics of each composite were essentially identical, exhibiting current-independent impedances of 0.2 Ω cm2 at 973 K. When the composites were calcined to 1373 K, the open-circuit impedances were much larger and showed a strong dependence on current density. The open-circuit impedances followed the ionic conductivities, with LSF– YSZ electrodes showing the lowest impedance and LCF–YSZ electrodes the highest. Scanning electron microscopy images and Brunauer–Emmett–Teller surface areas indicate that calcination at 1373 K causes the perovskites to form dense layers over the YSZ pores. A model is proposed in which diffusion of ions through the perovskite film limits the performance of the composite electrodes calcined at 1373 K.

 Reprinted in *Journal of the Electrochemical Society*, Volume 155, Issue 7, March 2008, pages B660-B665.
Publisher URL: http://www.ecsdl.org/dbt/dbt.jsp?KEY=JESOAN

Journal of The Electrochemical Society, **155** (7) B660-B665 (2008)
0013-4651/2008/155(7)/B660/6/$23.00 © The Electrochemical Society

The Effect of Ca, Sr, and Ba Doping on the Ionic Conductivity and Cathode Performance of $LaFeO_3$

F. Bidrawn,[a] S. Lee,[a,b] J. M. Vohs,[a,*] and R. J. Gorte[a,*,z]

[a]*Department of Chemical and Biomolecular Engineering, University of Pennsylvania, Philadelphia, Pennsylvania 19104, USA*
[b]*Korea Institute of Energy Research, Daejeon 305-343, Korea*

The influence of ionic conductivity on the performance of solid oxide fuel cell cathodes was studied for electrodes prepared by infiltration of 40 wt % $La_{0.8}Ca_{0.2}FeO_3$ (LCF), $La_{0.8}Sr_{0.2}FeO_3$ (LSF), and $La_{0.8}Ba_{0.2}FeO_3$ (LBF) into 65% porous yttria-stabilized zirconia (YSZ). The ionic conductivities of LCF, LSF, and LBF, measured between 923 and 1073 K using permeation rates in a membrane reactor, showed that LSF exhibited the highest ionic conductivities, followed by LBF and LCF. When electrodes were calcined to 1123 K, the performance characteristics of each composite were essentially identical, exhibiting current-independent impedances of 0.2 Ω cm^2 at 973 K. When the composites were calcined to 1373 K, the open-circuit impedances were much larger and showed a strong dependence on current density. The open-circuit impedances followed the ionic conductivities, with LSF–YSZ electrodes showing the lowest impedance and LCF–YSZ electrodes the highest. Scanning electron microscopy images and Brunauer–Emmett–Teller surface areas indicate that calcination at 1373 K causes the perovskites to form dense layers over the YSZ pores. A model is proposed in which diffusion of ions through the perovskite film limits the performance of the composite electrodes calcined at 1373 K.
 [DOI: 10.1149/1.2907431]

Manuscript submitted February 14, 2008; revised manuscript received March 12, 2008. Available electronically May 2, 2008.

Despite having a relatively high area specific resistance (ASR) at temperatures below 750°C, the standard solid oxide fuel cell (SOFC) cathode material with yttria-stabilized zirconia (YSZ) electrolytes is still a composite of Sr-doped $LaMnO_3$ (LSM) with YSZ. The ASR of cathodes made from mixed-conducting perovskites, such as Sr-doped $LaCoO_3$ (LSCo) or Sr-doped $LaFeO_3$ (LSF), can be much lower; unfortunately, this high performance tends to be unstable. In the case of LSCo, deactivation is almost certainly associated with solid-state reactions that form insulating phases, such as $La_2Zr_2O_7$, at temperatures as low as 700°C.[1] Because electrodes based on LSF deactivate after sintering at temperatures as low as 1000°C,[2-4] it is commonly assumed that similar solid-state reactions are responsible for deactivation in these electrodes as well.

However, deactivation by formation of insulating materials may not apply to LSF. Unlike the case with LSCo where X-ray diffraction (XRD) clearly shows the formation of new phases when LSCo and YSZ are in contact at 700°C, LSF–YSZ composites only show the formation of additional phases above 1400°C,[5] a temperature higher than that necessary to form insulating phases with LSM.[6] While the formation of additional phases is unlikely with LSF–YSZ electrodes at operating temperatures, it has been suggested that LSF reacts with YSZ to form a Zr-doped perovskite [e.g., $La_{0.8}Sr_{0.2}Fe_{0.9}Zr_{0.1}O_3$ (LSFZ)]. The evidence for this reaction comes from the observation that the perovskite lattice expands after the annealing of LSF–YSZ mixtures to 1200°C.[7] However, in addition to the fact that deactivation of LSF–YSZ cathodes occurs at significantly lower temperatures than that required to unequivocally form LSFZ, LSFZ is conductive, and an LSFZ–YSZ electrode prepared by infiltration exhibited good performance.[8]

In a study of the stability of LSF cathodes prepared by infiltration into porous YSZ from our laboratory, deactivation correlated with a loss of LSF surface area and the formation of what appeared to be a dense film of LSF covering the porous YSZ.[8] Impedance spectra also showed that the ohmic resistance of deactivated cells remained unchanged, a strong argument against the formation of insulating layers. Based on these observations, it was suggested that deactivation is either due to a decrease in O_2 adsorption rate (due to lost surface area) or to LSF forming an impenetrable barrier over the YSZ in the electrode. If LSF forms a dense layer, performance in the deactivated electrode could be limited by conduction of oxygen ions through the LSF.

* Electrochemical Society Active Member.
z E-mail: gorte@seas.upenn.edu

Because the ionic conductivity of $LaFeO_3$ likely depends on the dopant, we decided to compare the performance of Ca-, Sr-, and Ba-doped $LaFeO_3$ [$La_{0.8}Ca_{0.2}FeO_3$ (LCF), LSF, and $La_{0.8}Ba_{0.2}FeO_3$ (LBF)]. Previous work in which Ca, Sr, or Ba was doped on the A sites of $LaCo_{0.2}Fe_{0.8}O_3$ suggested that the ionic conductivities would decrease with dopant in the following order: Sr > Ba > Ca.[9,10] Whether this ordering of the ionic conductivities with dopant can be applied to the $LaFeO_3$ is uncertain, as are the absolute ionic conductivities of doped $LaFeO_3$. For example, Wiemhofer et al.[11] have reported that the ionic conductivity of $La_{0.8}Sr_{0.2}FeO_3$ at 973 K is 1.2×10^{-5} S/cm, while Patrakeev et al.[12] reported an ionic conductivity of 3.4×10^{-2} S/cm at 1023 K for this same material. A consequence of the higher conductivity reported by Patrakeev et al. would be to rule out the proposal that deactivation of LSF electrodes is associated with an impenetrable film, because the conductivity of YSZ at 1023 K is 2.9×10^{-2} S/cm.[13]

Therefore, we set out to measure the ionic conductivities of LCF, LSF, and LBF and to determine the performance of electrodes made with these three materials. What we show is that the ionic conductivities of the doped $LaFeO_3$ are low compared to that of YSZ and that the ordering of the ionic conductivities is as follows: LSF > LBF > LCF. For electrodes prepared by infiltration and calcination to 1123 K, the infiltrated perovskites are highly porous and electrode performance is similar for composites of YSZ with LSF, LBF, and LCF. However, when the infiltrated electrodes were calcined to 1373 K, the infiltrated perovskites formed dense films on the YSZ pores and performance increased with ionic conductivity.

Experimental

Ionic conductivities.— The samples used for measurements of both total and ionic conductivities were prepared from LCF, LSF, and LBF powders that were synthesized in our laboratory using the Pechini method.[8,14] Stoichiometric quantities of the nitrate salts were mixed with citric acid, with the concentration of citrate ions equal to that of the metal ions. After drying these solutions, the solids were heated to 1123 K to form the perovskite phases, formed into disk-shaped specimens, and finally sintered at 1773 K for 4 h in air. The calculated density of each specimen was greater than 92% of the theoretical density. XRD showed that each of the materials was single-phase. The positions of the (240) lines in the diffraction patterns, reported in Table I, are consistent with doping of Ca, Sr, and Ba.

Some disks were machined into bars, $3 \times 3 \times 10$ mm, and used to measure the total conductivities, σ_t, in air between 923 and

Table I. Peak positions for the (240) planes of doped $LaFeO_3$ samples used in the ionic conductivity measurements.

	$LaFeO_{3-d}$	LCF	LSF	LBF
2θ of (240) planes (degree)	57.40[a]	57.74	57.68	57.28

[a] Value reported from JCPDS 37-1493.

1073 K using four-probe measurements. The total conductivities of each material are listed in Table II and were found to be essentially independent of temperature over the measured range.

The ionic conductivities were determined by measuring the rate of oxygen permeation across the perovskite disks using a system shown diagrammatically in Fig. 1. For these measurements, the sample disks were machined to a diameter of 12 mm and a thickness between 3 and 3.6 mm and then attached to the end of a YSZ tube using leak-tight glass seals.[15] The oxygen permeating through each specimen was measured by balancing the steady-state permeation flux to the rate of oxygen pumped electrochemically across two Pt electrodes placed on opposite sides of the YSZ tube. The permeation fluxes were measured with the outside of the membrane exposed to air, while the $P(O_2)$ on the inside was allowed to vary between 5×10^{-7} and 2×10^{-2} atm. The difference in $P(O_2)$ across the membrane was determined using a second set of Pt electrodes on the YSZ tube.

For mixed-conducting membranes,[3] the permeation flux, j, is related to the bulk ambipolar conductivity, σ_{amb} [$\sigma_{amb} = \sigma_e\sigma_i/(\sigma_e + \sigma_i)$, where σ_e and σ_i are the electronic and ionic conductivities], by Eq. 1

$$\sigma_{amb} = \frac{16F^2L}{RT}\left[\frac{\partial j}{\partial \ln P(O_2)_{air}/P(O_2)_{in}}\right]_{P(O_2)_{in}\rightarrow P(O_2)_{air}} \quad [1]$$

In this equation, $P(O_2)_{air}/P(O_2)_{in}$ is the ratio of oxygen partial pressures, F is the Faraday constant, and L is the specimen thickness. The ionic conductivities are then calculated using Eq. 2

$$\sigma_i = \sigma_t\left[\frac{1}{2} - \frac{1}{2}\sqrt{1 - \frac{4\sigma_{amb}}{\sigma_t}}\right] \quad [2]$$

In the present paper, all of the ionic conductivities were calculated from data in which the $P(O_2)$ inside the system was between 2.5 and 3.9×10^{-2} atm.

Typical data relating the oxygen flux to the ratio of $P(O_2)$ across the membrane are shown in Fig. 2 for three different temperatures with the LBF sample. The reproducibility of this data and the stability of the perovskites to reduction during the course of the measurements were demonstrated by cycling the $P(O_2)$ inside the apparatus and showing that the relationship between oxygen flux and $P(O_2)$ remained unchanged. The linear relationship between the permeation flux and $P(O_2)_{air}/P(O_2)_{in}$, along with the strong temperature dependence of the flux, provides proof that the membranes were free of pinholes. Furthermore, we ruled out the possibility that the permeation fluxes were limited by surface-exchange kinetics. First, the zero intercept in Fig. 2 is inconsistent with surface-exchange limitations. Second, it has been estimated that the length scale for which the oxygen permeation flux is under mixed control of the surface exchange kinetics and bulk diffusion for LSF is approximately 0.3 mm,[16] a factor of 10 less than the thicknesses of our samples. Finally, we measured the oxygen permeation rate of the LSF specimen, the one exhibiting the highest fluxes, after coating the surfaces with Pt and showed that the addition of catalyst had no effect on oxygen fluxes.

Table II. Total conductivities of the doped $LaFeO_3$ samples as a function of temperature.

Specimen	923 K	973 K	1023 K	1073 K
LCF	56.7	56.8	57.5	58.7
LSF	79.9	79.7	78.9	77.8
LBF	49.6	51.1	51.9	51.8

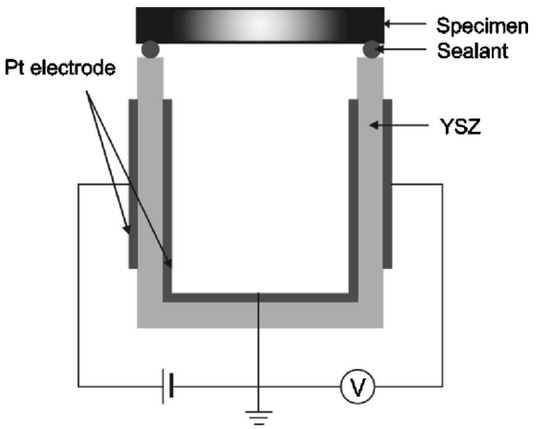

Figure 1. Schematic of the equipment used for measuring ionic conductivities.

Fuel cell measurements.— Fuel cells with composite cathodes formed by infiltration of LCF, LSF, and LBF into porous YSZ were prepared in a manner similar to that described elsewhere for LSF.[8,14] The first step in preparing the cells involved fabricating a circular YSZ wafer with two porous layers separated by a dense layer. In this study, the thickness of the dense layer varied from 100 to 125 μm (the variation was due to cells being made from different tapes), but the two porous layers were 10 and 50 μm thick in all cases. The diameter of the dense YSZ was 1.0 cm and the diameter of each porous layer was 0.67 cm. The porous-dense-porous wafers were prepared by laminating together three green tapes, with graphite pore formers included in the tapes for those layers requiring porosity. The tapes were fired to 1823 K for 4 h to produce the YSZ wafer, with porosities of 65% on both sides of the dense electrolyte.

The LCF–, LSF–, and LBF–YSZ composite cathodes were synthesized by infiltration of the 50 μm porous YSZ with aqueous solutions containing $La(NO_3)_3{\cdot}6H_2O$, $Fe(NO_3)_3{\cdot}9H_2O$, and either $Ca(NO_3)_2$, $Sr(NO_3)_2$, or $Ba(NO_3)_2$ at the proper molar ratios. The

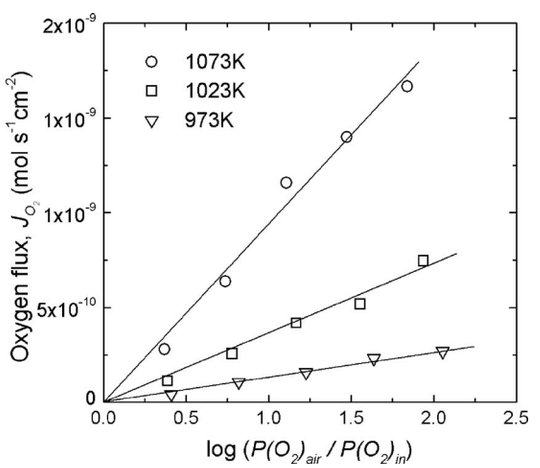

Figure 2. A plot of the oxygen permeation flux on the LBF specimen as a function of the oxygen partial pressure gradient.

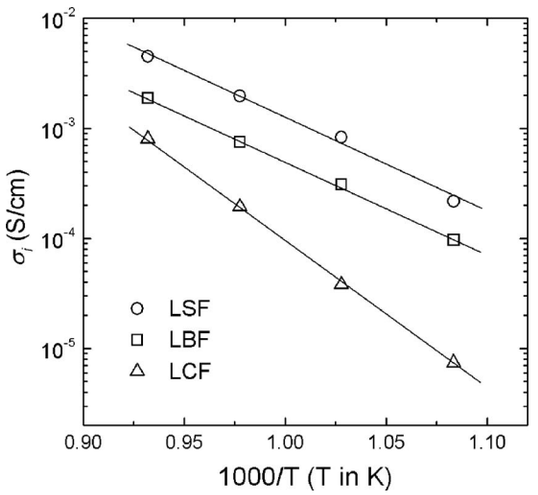

Figure 3. Ionic conductivities of the doped $LaFeO_3$ samples as a function of temperature.

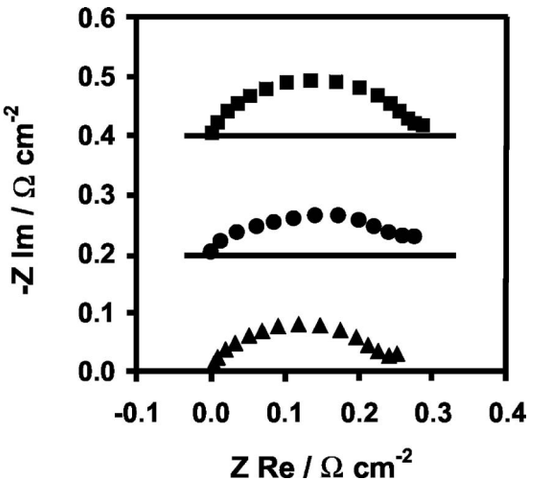

Figure 4. Open-circuit impedance data for cells made with LSF (■), LBF (●), and LCF (▲). The composite cathodes on each of these cells were calcined at 1123 K.

solutions also contained citric acid, with the concentration of citrate ions equal to that of the metal ions.[8,14] Infiltration steps were followed by calcination to 1123 K to remove the nitrate and citrate ions; multiple impregnation steps (approximately 10 for LSF and LCF and 20 for LBF) were used to reach a final loading of 40 wt % of the perovskite. Finally, some of the composites were calcined to 1373 K for 4 h to simulate deactivation, because an earlier study of LSF–YSZ cathodes showed that this high-temperature treatment led to similar performance changes to that observed after long-time fuel cell operation.[8] The physical characteristics of the cathode composites were examined by XRD, to ensure that the proper phases were produced, and by scanning electron microscopy (SEM).

The SOFC anodes were prepared from the 10 μm, porous YSZ layer by impregnating it with 40 wt % CeO_2 and 1 wt % Pd, again using the corresponding nitrate salts. Ag paste was then applied to the top of this layer for current collection. Based on earlier studies,[17,18] the performance characteristics of this anode at 973 K in humidified H_2 are described by an ohmic contribution of 0.08 Ω cm^2 and a nonohmic contribution of 0.1 Ω cm^2 for current densities below 1 A/cm^2. Because we have found the use of reference electrodes to be unreliable,[19] cathode performance in this paper was determined from the total-cell performance by subtracting the contribution of the above anode losses.

For fuel cell testing, the cells were attached to an alumina tube with a ceramic adhesive (Aremco, Ceramabond 552). Ag paste was used as the current collector under both air and fuel conditions. Impedance spectra were measured at open circuit in the galvanostatic mode with a frequency range of 0.1 Hz to 100 KHz and a 1 mA ac perturbation using a Gamry Instruments potentiostat. H_2 was introduced to the anode compartment at a flow rate of 50 mL/min through a room-temperature water bubbler for humidification.

Results and Discussion

Ionic conductivities.— The ionic conductivities of the LCF, LSF, and LBF are shown as a function of temperature in Fig. 3. As pointed out earlier, these values were measured with one side of the membrane at a $P(O_2)$ of 0.21 atm and the other between 2.5 and 3.9×10^{-2} atm, so that the measurements were under conditions similar to that experienced by an SOFC cathode. The absolute values for the conductivities of LSF, 8×10^{-4} S/cm at 973 K, lie between the previously reported values from Wiemhofer et al.,[11] 1.2×10^{-5} S/cm at 973 K, and Patrakeev et al.,[12] 3.4×10^{-2} S/cm at 1023 K. The differences in previously reported values may be due in part to the fact that the measurements were all performed at different $P(O_2)$. For example, Patrakeev et al. used the minimum in the total conductivity at low $P(O_2)$ as the ionic conductivity, clearly conditions far from 0.21 atm.

It is of interest to compare the conductivity of LSF to that of Sr-doped $LaCo_{0.2}Fe_{0.8}O_3$ (LSCF) because LSCF is presently being used by a number of groups in SOFC cathode applications.[20-23] Because LSCF is also one of the materials under consideration for oxygen-separation membranes, it is not surprising that significantly higher conductivities are reported for this material. For example, the ionic conductivity of $La_{0.6}Sr_{0.4}Co_{0.2}Fe_{0.8}O_3$ is 0.076 S/cm at 1073 K,[10] compared to the value of 0.0045 S/cm for LSF in our measurements. For SOFC applications, the conductivity of YSZ at 1073 K, 0.043 S/cm,[13] falls between these values.

Similar to what has been reported previously for Sr-, Ba-, and Ca-doped LSCF,[9,10] LSF exhibited the highest ionic conductivity, followed by LBF and LCF. This is likely related to Sr^{+2} ions having the optimum size for movement of ions in the $LaFeO_3$ lattice. As expected, the ionic conductivities for each material exhibited an Arrhenius temperature dependence. The activation energies for ionic transport of LSF and LBF were nearly the same, 0.77 eV (0.779 eV for LSF and 0.763 eV for LBF), while the activation energy for LCF was significantly larger, 1.2 eV. These values are also in reasonable agreement with activation energies for ionic conduction determined with doped LSCF.[10]

Cathode performance characteristics.— When the LSF, LBF, and LCF composites were calcined to only 1123 K, the fuel cells based on these cathodes showed cell potentials that decreased linearly with current density at 973 K. (These measurements were performed with the anode exposed to humidified H_2 and the cathode exposed to air.) Because of the linearity of the voltage–current density (*V-i*) curves, the open-circuit impedance plots in Fig. 4 are sufficient to describe cell performance. The ohmic losses have been removed from the impedance curves because the electrolyte thickness varied between 100 and 125 μm; however, ohmic impedances were between 0.65 and 0.8 Ω cm^2 for each cell, values consistent with that expected for this electrolyte thickness at 973 K, plus the contribution of the anode.[17,18] The data in Fig. 4 show that the performance of each cathode was essentially identical, independent of which dopant was added to $LaFeO_3$. Each of the cells showed nonohmic losses between 0.25 and 0.3 Ω cm^2. Because the anode contributes approximately 0.1 Ω cm^2 to this value,[17,18] each of the cathodes contributes between 0.15 and 0.2 Ω cm^2. Previously,

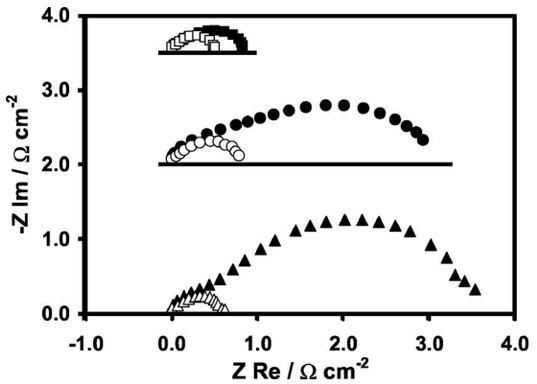

Figure 5. Impedance data for cells made with LSF (■), LBF (●), and LCF (▲). The composite cathodes on each of these cells were calcined at 1373 K. The filled symbols show data measured at open circuit, while the open symbols were obtained at a current density of 100 mA/cm^2.

losses for LSF–YSZ cathodes, prepared by infiltration and calcined to 1123 K, had been estimated to be between 0.1 and 0.15 Ω cm^2 for cathode-supported cells.[8,14] The losses in this study were similar.

When the composite cathodes were calcined to 1373 K, to simulate deactivation,[8] the cell performances were much worse. (Note: The calcination to 1373 K was performed prior to adding the anode or Ag current collectors, so performance differences can only be due to changes in the cathodes.) The decreased performances do not appear to be due to solid-state reactions between the perovskites and the YSZ. First, XRD measurements on the composites heated to 1373 K showed no evidence for new phases other than that of the perovskite and YSZ. Also, none of the composites showed evidence for a lattice expansion of the perovskite phase, a result which would indicate diffusion of Zr ions into the perovskite.[7] Finally, the ohmic losses for the cells heated to 1373 K were again between 0.65 and 0.8 Ω cm^2, depending on the electrolyte thickness. A decreased conductivity of the perovskite phase or formation of new insulating phases would be expected to increase the ohmic losses.

Performance differences following the 1373 K calcination were associated with the nonohmic components of the impedances, as shown in Fig. 5. First, based on the open-circuit impedances, the three doped-$LaFeO_3$ cathodes were no longer identical. The LSF–YSZ cathodes exhibited the lowest losses, followed by the LBF–YSZ and LCF–YSZ cathodes. Second, the nonohmic losses on each of the composite cathodes exhibited a strong dependence on the current density after heating to 1373 K, similar to what had been reported earlier with infiltrated LSF composites.[8] The nonohmic component of the impedance curve for the cell with the LSF–YSZ cathode decreased from 1.0 Ω cm^2 at open circuit to 0.5 Ω cm^2 at a current density of 100 mA/cm^2. The decrease in impedance with current was even more dramatic with the cells having LCF–YSZ and LBF–YSZ cathodes. The nonohmic impedances decreased from 3.5 Ω cm^2 at open circuit to 0.6 Ω cm^2 at 100 mA/cm^2 on the cell with the LCF–YSZ cathode and from 3.0 Ω cm^2 at open circuit to 0.8 Ω cm^2 at 100 mA/cm^2 on the cell with the LBF–YSZ cathode.

Structural characterization.— As discussed above, we found no evidence by XRD that solid-state reactions are responsible for the changes in electrode performance following calcination to 1373 K. Therefore, to understand the reasons for the changes that were observed, we examined each of the perovskite composites using SEM and Brunauer–Emmett–Teller (BET) isotherms,[24] before and after the high-temperature treatment, with the results shown in Fig. 6 and Table III.

Prior to the addition of the perovskites, the YSZ scaffold has relatively uniform pores, between 1 and 10 μm in diameter, as shown in Fig. 6a.[8] The surfaces of the pores are smooth, with some areas showing well-defined crystallographic facets. After the addition of LSF, LBF, and LCF and calcination to 1123 K, Fig. 6b, d, and f, the surface of the pores are coated with small, partially sintered, perovskite particles, approximately 0.05–0.1 μm in size. The sintering is more complete with the LBF sample, probably because this sample required more infiltration steps to achieve the 40 wt % loading, due to the low solubility of Ba ions. With each of the perovskites, the particles form a well-connected network, which helps to explain the good conductivity of the infiltrated composite; but this network appears to have sufficient porosity to allow oxygen to diffuse to the YSZ interface. The high porosity is also demonstrated by the BET measurements. While the initial YSZ scaffold had a specific surface area of 0.40 m^2/g, the surface areas of the infiltrated composites were significantly higher after calcination to 1123 K, ranging from 0.95 m^2/g for the LBF–YSZ composite to 1.69 m^2/g for the LSF–YSZ composite.

After heating the composites to 1373 K, the perovskite particles form dense films over the YSZ pore structure, as shown in Fig. 6c, e, and g. That these films had low porosity was also established by the BET data. The surface areas of the composites ranged from 0.41 to 0.43 m^2/g, values that were similar to that of the initial YSZ scaffold.

We suggest that the changes in the performance of the electrodes following calcination to 1373 K are associated with the formation of the dense film of the perovskite and that the performance of the electrodes calcined to 1373 K is limited by ionic diffusion through that film, as illustrated in Fig. 7. When the electrodes were calcined to only 1123 K, there is sufficient porosity for O_2 to diffuse close to the YSZ interface, where it can then react at three-phase boundary sites to form oxygen ions, which in turn are transported to the electrolyte by the YSZ scaffold. After calcination to 1373 K, the O_2 must react on the surface of the perovskite, with the ions diffusing through the perovskite film to the YSZ scaffold.

This model explains several observations quite well. First, it is consistent with the absence of solid-state reactions. Second, the open-circuit impedances of the cathodes based on LSF, LBF, and LCF are nearly identical when calcined to only 1123 K. The differences in the ionic conductivities of the highly porous perovskite are irrelevant in this case, because gas-phase oxygen can approach the perovskite–YSZ interface. After calcination, the electrode performance is limited by diffusion of ions and the open-circuit impedance scales with the ionic conductivity. LSF has the highest ionic conductivity, and the LSF–YSZ cathode exhibits the lowest impedance.

Second, the picture in Fig. 7 may help to explain the dependence of the impedance on current density. Within the cathodes calcined at 1373 K, there are two relevant diffusion processes: (*i*) diffusion of oxygen ions through the YSZ in the scaffold to the electrolyte and (*ii*) diffusion of oxygen ions through the perovskite film. Because the walls of the YSZ scaffold are relatively thick compared to the perovskite film thickness and because the ionic conductivity of YSZ at 973 K is 20 times that of LSF and nearly 500 times that of LCF, it is likely that the oxygen chemical potential within the YSZ is a function only of the distance from the electrolyte. Imposition of a current causes a chemical potential gradient across the perovskite film, but the chemical potential difference depends on the distance from the electrolyte. The coupling of these two diffusion processes would then lead to the nonlinearity in the *V-i* curves. Obviously, we cannot rule out the possibility that high-temperature calcination changes the surface areas of the doped perovskites, which in turn affects adsorption rates; however, that model certainly does not explain all of the observations as well.

The model illustrated in Fig. 7 has a number of implications for stabilizing the infiltrated electrodes based on $LaFeO_3$. First, one would expect to see significant improvements if the ionic conductivity of the perovskite could be increased even modestly, so long as the dopants that were used to achieve higher ionic conductivity were unreactive with the YSZ. That is probably not true for Co (LSCF), because there is evidence of solid-state reactions between YSZ and Co-doped LSM.[25] Another approach to achieving higher performance would be to use thinner perovskite films. The difficulty in

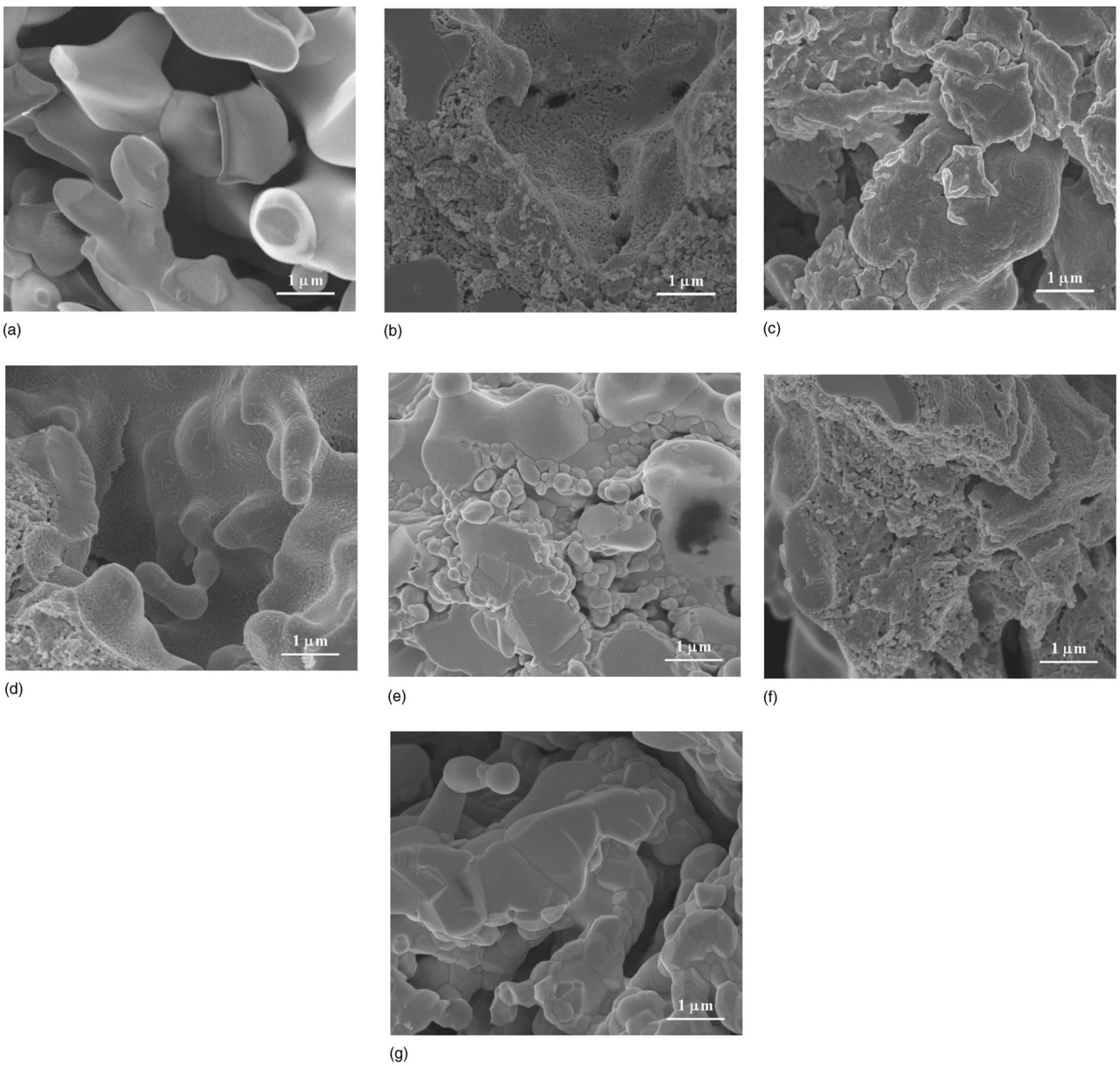

Figure 6. (a) An SEM micrograph showing the structure of the porous YSZ scaffold. (b) An SEM micrograph of the electrode following infiltration of 40 wt % LSF and calcination to 1123 K. (c) An SEM micrograph of the electrode following infiltration of 40 wt % LSF and calcination to 1373 K. (d) An SEM micrograph of the electrode following infiltration of 40 wt % LBF and calcination to 1123 K. (e) An SEM micrograph of the electrode following infiltration of 40 wt % LBF and calcination to 1373 K. (f) An SEM micrograph of the electrode following infiltration of 40 wt % LCF and calcination to 1123 K. (g) An SEM micrograph of the electrode following infiltration of 40 wt % LCF and calcination to 1373 K.

Table III. Surface areas measured from BET isotherms, performed using Kr at 78 K.

YSZ scaffold	0.40 m^2/g
LSF calcined at 1123 K	1.69
LBF at 1123 K	0.95
LCF at 1123 K	1.59
LSF at 1373 K	0.43
LBF at 1373 K	0.41
LCF at 1373 K	0.43

this approach is that maintaining high electronic conductivity may be hard with lower perovskite loadings, although this approach may be possible with careful tuning of the YSZ pore structure. Finally, if one could prevent loss of the pore structure that is present after low-temperature calcination, it may be possible to stabilize the initial high performance.

Perhaps the most important conclusion of this and a previous study of LSF–YSZ cathodes[8] is that the mechanism for deactivation of cathodes may well be different for different materials, and well-established deactivation mechanisms for $LaCoO_3$-based electrodes may not apply to other systems. This opens up new strategies for the development of highly stable, high-performance SOFC cathodes.

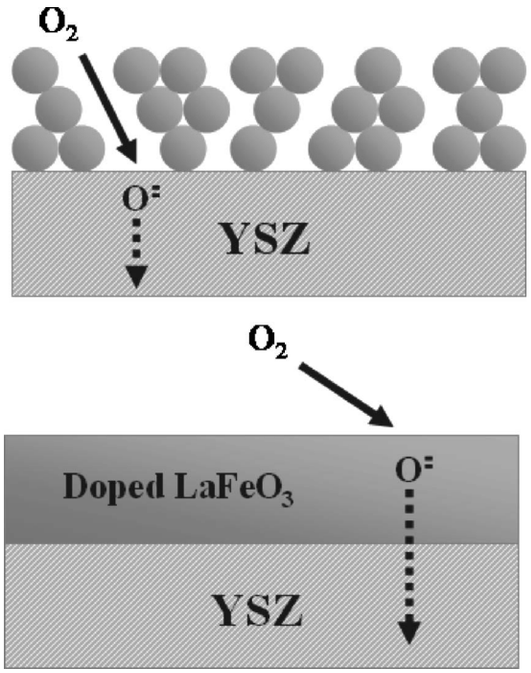

Figure 7. A schematic illustrating the effect of higher temperature calcination on the infiltrated, doped $LaFeO_3$. The upper picture represents the situation following calcination at 1123 K and the lower represents 1373 K.

Conclusions

Composite cathodes formed by infiltration of doped $LaFeO_3$ into YSZ tend to form dense perovskite films over the porous YSZ structure at higher calcination temperatures. This dense film limits the performance of the electrodes due to the relatively low ionic conductivity of the $LaFeO_3$ perovskites. Strategies for stabilizing the LSF–YSZ electrodes should target ways to avoid the formation of a thick layer of LSF near the three-phase boundary.

Acknowledgment

This work was funded by the U.S. Department of Energy's Hydrogen Fuel Initiative (grant no. DE-FG02-05ER15721).

University of Pennsylvania assisted in meeting the publication costs of this article.

References

1. M. Sase, D. Ueno, K. Yashiro, A. Kaimai, T. Kawada, and J. Mizusaki, *J. Phys. Chem. Solids*, **66**, 343 (2005).
2. S. P. Simner, J. F. Bonnett, N. L. Canfield, K. D. Meinhardt, V. L. Sprenkle, and J. W. Stevenson, *Electrochem. Solid-State Lett.*, **5**, A173 (2002).
3. S. P. Simner, J. F. Bonnett, N. L. Canfield, K. D. Meinhardt, J. P. Shelton, V. L. Sprenkle, and J. W. Stevenson, *J. Power Sources*, **113**, 1 (2003).
4. S. P. Simner, M. D. Anderson, J. F. Bonnett, and J. W. Stevenson, *Solid State Ionics*, **175**, 79 (2004).
5. J. Hole, D. Kuseer, M. Hrovat, S. Bernik, and D. Kolar, *Solid State Ionics*, **95**, 259 (1997).
6. N. Q. Minh, *J. Am. Ceram. Soc.*, **76**, 563 (1993).
7. S. P. Simner, J. P. Shelton, M. D. Anderson, and J. W. Stevenson, *Solid State Ionics*, **161**, 11 (2003).
8. W. Wang, M. D. Gross, J. M. Vohs, and R. J. Gorte, *J. Electrochem. Soc.*, **154**, B439 (2007).
9. S. Li, W. Jin, P. Huang, N. Xu, J. Shi, Y. S. Lin, M. Z.-C. Hu, and E. A. Payzant, *Ind. Eng. Chem. Res.*, **38**, 2963 (1999).
10. J. W. Stevenson, T. R. Armstrong, R. D. Carneim, L. R. Pederson, and W. J. Weber, *J. Electrochem. Soc.*, **143**, 2722 (1996).
11. H.-D. Wiemhofer, H.-G. Bremes, U. Nigge, and W. Zipprich, *Solid State Ionics*, **150**, 63 (2002).
12. M. V. Patrakeev, J. A. Bahteeva, E. B. Mitberg, I. A. Leonidov, V. L. Kozhevnikov, and K. R. Poeppelmeier, *J. Solid State Chem.*, **172**, 219 (2003).
13. K. Sasaki and J. Maier, *Solid State Ionics*, **134**, 303 (2000).
14. Y. Huang, J. M. Vohs, and R. J. Gorte, *J. Electrochem. Soc.*, **151**, A646 (2004).
15. P. R. Shah, T. Kim, G. Zhou, P. Fornasiero, and R. J. Gorte, *Chem. Mater.*, **18**, 5363 (2006).
16. T. Ishigaki, S. Yamauchi, K. Kishio, J. Mizusaki, and K. Fueki, *J. Solid State Chem.*, **73**, 179 (1998).
17. M. D. Gross, J. M. Vohs, and R. J. Gorte, *J. Electrochem. Soc.*, **154**, B694 (2007).
18. M. D. Gross, J. M. Vohs, and R. J. Gorte, *Electrochem. Solid-State Lett.*, **10**, B65 (2007).
19. S. McIntosh, J. M. Vohs, and R. J. Gorte, *J. Electrochem. Soc.*, **150**, A1305 (2003).
20. S. P. Simner, M. D. Anderson, M. H. Engelhard, and J. W. Stevenson, *Electrochem. Solid-State Lett.*, **9**, A478 (2006).
21. A. Esquirol, N. P. Brandon, J. A. Kilner, and M. Mogensen, *J. Electrochem. Soc.*, **151**, A1847 (2004).
22. J. M. Serra and H.-P. Buchkremer, *J. Power Sources*, **172**, 768 (2007).
23. W.-H. Kim, H.-S. Song, J. Moon, and H.-W. Lee, *Solid State Ionics*, **177**, 3211 (2006).
24. Y. Huang, J. M. Vohs, and R. J. Gorte, *J. Electrochem. Soc.*, **152**, A1347 (2005).
25. Y. Huang, J. M. Vohs, and R. J. Gorte, *J. Electrochem. Soc.*, **153**, A951 (2006).